11th International Symposium on Turbulence and Shear Flow Phenomena (TSFP11)
Southampton, UK, July 30 to August 2, 2019

TOWARDS A ONE-DIMENSIONAL TURBULENCE APPROACH FOR ELECTROHYDRODYNAMIC FLOWS

Juan A. Medina Mendez, Heiko Schmidt
Chair of Numerical Fluid and Gas Dynamics
BTU Cottbus-Senftenberg
Siemens-Halske-Ring 14, D-03046 Cottbus, Germany
medinjua@b-tu.de, schmidth@b-tu.de

Ulrich Riebel
Chair of Particle Technology
BTU Cottbus-Senftenberg
Burger Chaussee 2, LG 4/3, D-03044 Cottbus, Germany
riebel@b-tu.de

ABSTRACT

The One-Dimensional Turbulence model is modified in this work for its application to a classical electrohydrodynamic (EHD) problem. Being the first study case, this work is focused on the influence of electrostatic fields and space charge on the velocity field inside a wire-plate Electrostatic Precipitator (ESP) with one-way-coupling dynamics. The study case is an attempt to replicate velocity profiles and Turbulent Kinetic Energy (TKE) budgets obtained in the Direct Numerical Simulation (DNS) carried out by Soldati and Banerjee (1998). Qualitative trends are confirmed in preliminary ODT results, thus showing the potential of the stochastic ODT modeling approach for other types of EHD flows.

GENERAL CONSIDERATIONS ON NUMERICAL EHD FLOW MODELLING

Electrostatic precipitation is highly appealing in the industry due to its uses in flue gas purification or chemical manufacture. Adamiak (2013) offers a formidable literature review on numerical models in ESP research. In general, the limited understanding and unavailability of proper closure models for electrohydrodynamic (EHD) flows makes numerical simulation research largely dependant on Direct Numerical Simulation (DNS) methods.

In order to understand part of the interactions that may occur in EHD flows, as well as some modelling considerations, we refer to a general definition of the electrical current density $\vec{J}$ from Panofsky & Phillips (2005). Neglecting magnetic contributions to the electric current, we can define for the simple case of current generated by pure ionic charges,

$$\vec{J} = \rho_f \vec{V} + b\vec{E}\rho_f + \frac{\partial \vec{P}}{\partial t} \tag{1}$$

The first term in the right hand side (RHS) of Eq. (1) is the convective current of the free charge. It is normally granted that the velocity of the ions is significantly larger than the flow velocity, $\vec{V}_{ions} \gg \vec{V}$, and therefore, the convective term can be ignored in leading order. We refer to this asymptotic limit as a one-way-coupling dynamic, as in Soldati & Banerjee (1998). The second term in the RHS of Eq. (1) is the true current, given by the charge collisions and the drift velocity of the charges. Here, b is the ionic mobility coefficient, ρ_f is the ionic charge density and $\vec{E}$ is the electric field produced by the charge distribution. Finally, the last term refers to the electric polarization current, given by the rate of change of the electric polarization vector $\vec{P}$. This term can be ignored in fluids with very low electric susceptibility, such as air.

Soldati & Banerjee (1998) were pioneers in the application of DNS to study one-way-coupled EHD flow fields in ESPs. After Soldati and Banerjee, EHD flow research achieved yet another important milestone when Schmid & Vogel (2003) discussed and analyzed Eulerian and Lagrangian approaches for modelling particle transport in ESPs. Recently, the first closure modeling for EHD flows using a Reynolds Stress Model (RSM) was introduced by Kourmatzis & Shrimpton (2018). Closure models for EHD flows are challenging due to the highly non-linear nature of the TKE budget term $\overline{\vec{V}' \cdot \vec{J}'}$, which is the mean rate at which the electric body force (EBF) contributes energy to the turbulence (see Davidson & Shaughnessy (1986)).

In this work, we pursue an alternative stochastic approach to study EHD flows. The One-Dimensional Turbulence (ODT) model is a neat and relatively accessible 1-D stochastic turbulence model, which works in an operator splitting fashion for turbulent advection and molecular diffusion (see Kerstein (1999)). Since this work is the first application of ODT in EHD flows, we focus on a validation of the newly proposed approach with the DNS data from Soldati & Banerjee (1998). For that, we discuss first the new modelling considerations. Traditional ODT formulation aspects are not discussed here. These can be found elsewhere, e.g. Ashurst & Kerstein (2005) and Lignell *et al.* (2013). The case set-up and simulation parameters are presented

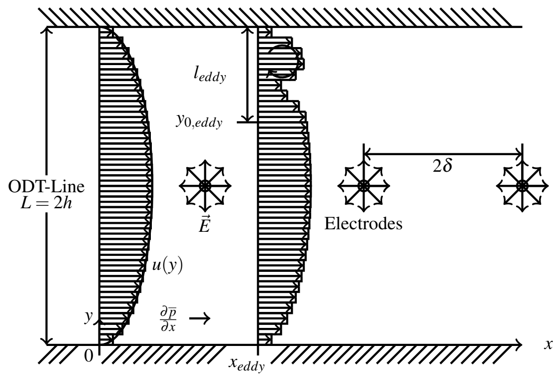

Figure 1: Sketch description of an eddy event taking place at a certain position in the flow within an ESP.

afterwards. Simulation results are then analyzed from the point of view of the validation of the model, as well as a focus on small physical insights on turbulent transport which can be straightforwardly obtained with ODT. Finally, we give some closing remarks regarding the applicability of the model and a brief outlook on future research opportunities.

ODT MODEL FOR ONE-WAY-COUPLED EHD FLOWS

Eddy events, which represent effects of turbulent advection on a 1-D domain, are selected following a statistical Poisson process involving the position and the length of an eddy, y_0 and l, respectively. Every eddy deemed energetically plausible by its calculated rate λ provokes a deterministic advancement process, as in Lignell *et al.* (2013). This operation involves the temporal (T-ODT) or spatial (S-ODT) advancement of deterministic ODT evolution equations. T-ODT and S-ODT formulations construct, therefore, eddy rates of the shape $\lambda(y_0, l, t)$ or $\lambda(y_0, l, x)$, respectively. In this work, we focus on the S-ODT advancement. This takes place from a starting position x_0 to a position $x_0 + \sum \Delta x_{sampling}$ at the position of an implemented eddy, where $\sum \Delta x_{sampling}$ is a sequence of spatial streamwise sampling ratios which results in a) an eddy implementation followed by a subsequent deterministic advancement, or b) exceeding a pre-defined advancement threshold, thus triggering a deterministic advancement.

The ODT model implementation in a wire-plate ESP is shown in Figure 1. It shows an eddy taking place at a location x_{eddy}. Wire-electrodes are located in a periodic array configuration with a wire-to-wire distance of 2δ. The ODT line spans the cross-width h of the channel.

The characteristic mapping process of eddy events, the triplet map function $f(y)$ as in Kerstein (1999), is measure preserving. For a one velocity component framework, this implies conservation of mass, momentum and energy in an incompressible flow. So far, it has only been possible to consistently state a vector formulation in S-ODT, i.e. with three velocity components, in the case of boundary layer type flows, e.g. Ashurst & Kerstein (2005) and Lignell *et al.* (2013). Therefore, given that the flow evaluated in this work is a channel flow type, we only solve for one velocity component in our S-ODT formulation, i.e. the streamwise velocity component u.

In contrast with the eddy events, mass conservation in 1-D is trivially satisfied during the deterministic advancement due to the incompressibility condition, i.e. constant density in the fixed size system. It is also possible to simultaneously enforce a balance on the streamwise momentum flux, which coincides with the kinetic energy of the system, by solving the conservative form of the streamwise momentum equation,

$$\frac{\partial \rho u^2}{\partial x} = -\frac{\partial \overline{p}}{\partial x} + \frac{\partial}{\partial y}\left(\mu \frac{\partial u}{\partial y}\right) \tag{2}$$

Here, the first term on the right hand side (RHS) of the equation, $\partial \overline{p}/\partial x$, is a mean pressure gradient driving the flow. The second term on the RHS is the relevant component of the viscous stress tensor. ρ and μ symbolize the constant density and dynamic viscosity of the flow, respectively. Note that the kinematic viscosity is $\nu = \mu/\rho$. In order to model the EHD effects on the flow, the volumetric EBF $\rho_f \vec{E}$ would be required, as in Soldati & Banerjee (1998). In our model, adding an external body force term in Eq. (2) implies not only the corresponding change in the momentum of the flow, as in the DNS, but also a change in the kinetic energy. The latter is not a problem in the DNS given that mass and energy conservation are enforced by guaranteeing the zero divergence of the 3-D velocity field. However, this is not feasible in ODT. In fact, in contrast to the inherent 3-D boundary value problem (elliptic) solved by DNS, S-ODT solves a parabolic flow (see Ashurst & Kerstein (2005) for details). Even solving a 2-D divergence condition induces an elliptic character on the flow. Therefore, we can only impose a 1-D zero divergence condition on the velocity field, i.e., $\partial v/\partial y = 0$, where v is the crosswise or wall-normal velocity component. This clarifies the absence of the advective term in Eq. (2) given that $v = 0$ everywhere due to the imposed zero gradient condition and the no-slip condition at the wall.

In order to incorporate the effects of the EBF, we refer to the decomposition of the current density onto its solenoidal and irrotational components suggested by Davidson & Shaughnessy (1986). The irrotational component must be neglected in our model, since it is coupled with the 3-D pressure gradient force acting on the flow. The solenoidal component should be considered instead, since it is responsible for the turbulence and vortical interactions. By approximating the current density vector in the one-way coupled regime with constant ionic mobility, we can suggest a simple decomposition of the current density vector as follows,

$$\vec{J} \approx b\vec{E}\rho_f = \nabla\left(-b\phi\rho_f\right) + b\phi\nabla\rho_f \tag{3}$$

This decomposition is based on an algebraic identity and the relation,

$$\vec{E} = -\nabla\phi \tag{4}$$

ϕ is the electrostatic potential in Eq. (4). This decomposition allows us to find a (non-unique) irrotational component of $\vec{J}$, $\nabla\left(-b\phi\rho_f\right)$. We interpret the remaining part of $\vec{J}$ as the solenoidal component, $b\phi\nabla\rho_f$. Note that this decomposition is applicable given that our sole purpose is the subtraction of the effects of an (arbitrary) irrotational contribution to the current, which we have empirically found to be responsible of negative velocities in the flow, effectively violating the assumptions required in the S-ODT formulation.

The streamwise rotational component of $\vec{J}$, i.e. $b\phi\partial\rho_f/\partial x$, can be used as a variable body force distribution in Eq. (2). The wall-normal rotational component, $b\phi\partial\rho_f/\partial y$, should be used during eddy events to influence the turbulent transport. The latter is done in this work by a mechanism to model the EHD instability.

The modelling of the EHD instability is based on a previously published ODT mechanism for affecting the probability of selection of eddy events, the ODT Darrieus-Landau instability formulation from Jozefik *et al.* (2015). This is a formal pathway in ODT to reproduce the dynamics of 3-D instabilities, which can not be directly captured, but are responsible for turbulence generation or decay. To replicate the effects of the EHD instability (as in Atten *et al.* (1987)), we resort to the generation of an equivalent external force utilizing the D'Alembert Principle. The rotational component of $\vec{J}$ involved in the EBF can be analyzed analogous to Jozefik *et al.* (2015), in which there is a gradient field $a = \partial\phi/\partial y = E_y$ associated to the force responsible for causing the instability, which acts upon a background (charge) density field. The change in energy associated with the perturbations produced by influence of the ODT eddies, characterized by $f(y)$ and the kernel function $K(y) = y - f(y)$, can then be defined as,

$$E_{EHD} = -\frac{K_0}{l^3}\int_{y_0}^{y_0+l} u[f(y)]K(y)\frac{j_y'[f(y)]}{b}\mathrm{d}y \tag{5}$$

Here, the gradient field is coupled to the charge density fluctuations, resulting in the evaluation of perturbations in the mapped wall-normal current density $j_y'[f(y)]/b = j_y[f(y)]/b - \overline{j_y}/b$, where $\overline{j_y}$ is an average of the current density over the eddy range, l. Note that Eq. (5) actually refers to an energy flux calculation, as required by the S-ODT formulation (see Ashurst & Kerstein (2005)).

In order to clarify the appearance of the factor K_0/l^3, we refer to the definition of the eddy turnover time in ODT used in this work, which is equivalent to the one used in Ashurst & Kerstein (2005). The definition $K_0 = \int_{y_0}^{y_0+l} K^2\mathrm{d}y$ is applied, which is equal to $4l^3/27$ in the continous limit. The eddy turnover time τ counterpart in S-ODT is ξ. This is a turnover characteristic length $\xi = \widetilde{u}\tau$, which is modelled based on the scaling of the available eddy kinetic energy flux Q'', as

$$Q'' \sim \frac{1}{2}\frac{\int_{y_0}^{y_0+l}\rho u K^2\mathrm{d}y}{\tau^2} = \frac{\widetilde{u}^2}{2}\frac{\int_{y_0}^{y_0+l}\rho u K^2\mathrm{d}y}{\xi^2} \tag{6}$$

In Eq. (6), $\widetilde{u}$ is the density weighted (Favre-averaged) velocity in the eddy range. Due to our one-component formulation, the available eddy kinetic energy flux is $Q'' = Q$, where Q is the extractable energy flux of the streamwise velocity component, defined according to the spatial formulation from Ashurst & Kerstein (2005). The correct scaling of the eddy turnover time (see Ashurst & Kerstein (2009) for details) is then based on Q'' and a viscous penalty factor formulated entirely on dimensional grounds as $E_{vp} \sim \rho\widetilde{u}\nu^2/l$. Adding our EHD potential energy flux contribution to the definition of ξ in Ashurst & Kerstein (2009), results in,

$$\frac{\widetilde{u}^2}{2}\frac{\int_{y_0}^{y_0+l}\rho u K^2\mathrm{d}y}{\xi^2} = \frac{K_0}{l^3}\left(\frac{K_0}{l^3}Q'' - \frac{Z}{2}E_{vp} + E_{EHD}\right) \tag{7}$$

With Eq. (7), it is now easy to see the justification for the factor K_0/l^3 in the E_{EHD} term. K_0/l^3 is just a factor for consistency in the scaling of E_{EHD} with respect to Q''.

The eddy rate parameter λ, which deems an eddy as energetically feasible or not for implementation, is also formulated on the grounds of dimensional analysis, i.e.

$$\lambda = \frac{C}{l^2\xi} \tag{8}$$

In Equations (7) and (8), C and Z are both constants of proportionality. These are the 2 ODT model parameters recognized in all ODT publications. These parameters must be calibrated for a specific flow configuration.

CASE SET-UP

In an attempt to replicate the DNS results from Soldati & Banerjee (1998) with ODT, we utilize the same geometry and considerations as in the DNS. The investigated flow is a channel flow forced by a mean pressure gradient, which is subject to an external electrical body force, in a one-way-coupling dynamic. That is, the electric field affecting the flow is always the same, and can be calculated beforehand. The electric field is generated by an infinitely long linear array of point electrodes, which operate at a discharge voltage $\phi_{electrode}$. The collector plates (walls of the channel) are grounded at a voltage $\phi_{plate} = 0$. The calculation of the electrostatic field follows the method in Yamamoto (1979) for the three-wire configuration, which only solves for a quarter of the region adjacent to an electrode due to symmetry. The normal electric field across all symmetry lines is 0. The tangential electric field at the collector plate is also 0.

The electrostatic fields are calculated by solving the 2-D Maxwell equations in the electroquasistatic approximation,

$$\nabla\cdot\vec{E} = \frac{\rho_f}{\varepsilon_0} \tag{9}$$

$$\nabla\cdot\vec{J} = 0 \tag{10}$$

Here, we have used the total 2-D current density definition in the one-way coupled regime from Eq. (3), $b\vec{E}\rho_f$, as well as the electrostatic potential relation given by Eq. (4). In Eq. (9), ε_0 is the electric permittivity of the vacuum. The calculations consider the value of ionic mobility for positive discharge in air, $b = 1.4311\times10^{-4}\mathrm{m}^2/(\mathrm{Vs})$.

As in Yamamoto (1979), the equations are solved with a Finite Difference (FD) method discretization, where the linear current density measured at the plate (I_{plate}) is used as a stopping criteria for the iteration procedure evaluating ϕ and ρ_f. All variables obtained at the nodes with the FD method are interpolated to cell centers in the cross-wise direction in order to use them in the ODT lines. Since the channel is infinite (periodic) in streamwise direction, a given discrete section of the channel is reused as many times as needed during an ODT simulation. Figure 2 shows the distribution of the electrostatic potential for the high voltage case. The required parameters for the calculation of the electrostatic field can be found in Table 1.

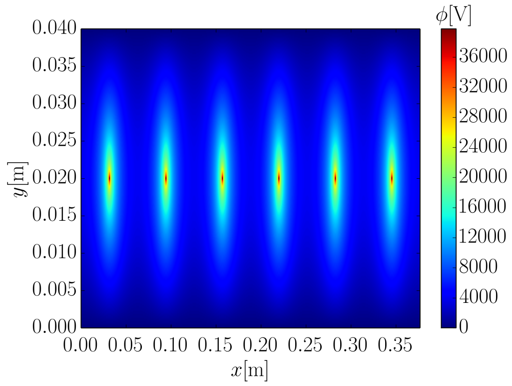

Figure 2: Distribution of the electrostatic potential in the ESP for case B. The channel height is $2h = 0.04$m.

Table 1: Electrostatic field parameters for the different cases investigated. The channel height is $2h$ and the wire-to-wire distance is 2δ.

Case	δ [m]	h [m]	$\phi_{electrode}$ [V]	ϕ_{plate} [V]	I_{plate} [mA/m]
A	0.0314	0.02	32000	0	0.30
B	0.0314	0.02	42000	0	0.75

The flow simulations can be started once the electrostatic field is computed. ODT model parameters C and Z are calibrated for the pure incompressible channel flow without EHD effects (case 0 in Table 2), and are expected to remain fixed afterwards for the evaluation of the low and high voltage cases (A and B, respectively, as in Tables 1 and 2). An exception to this rule will be discussed afterwards. Although there are already quantitative differences in the channel flow calibration case without EHD effects (not shown here), we choose the parameter values $C = 1.5$ and $Z = 100$ as those who are able to provide a good qualitative agreement with the incompressible mean velocity profiles of the pure channel flow. ODT simulations require, additionally, the information regarding the Kolmogorov length scale η and a cutoff length scale as an input for the assumed PDF of eddy sizes, as detailed by Lignell *et al.* (2013). The cutoff length scale, L_{max}, is in this case the characteristic length of the channel, i.e. half of the channel width. The simulations shown in this work were run with a dynamic mesh adaption procedure, as in Lignell *et al.* (2013). The deterministic advancement between eddy events in ODT is achieved by solving Eq. (2) with the added streamwise rotational current density term $\phi\partial\rho_f/\partial x$. Note that this is a quadratic PDE for u, which is solved using an iterative method for the calculation of the square root of u^2. The parameters for ODT simulations can be found in Table 2. Air properties $\nu = 1.66 \times 10^{-5}\mathrm{m}^2/\mathrm{s}$ and $\rho = 1.38\mathrm{kg/m}^3$ were used, as in Soldati & Banerjee (1998).

Table 2: Simulation parameters and obtained bulk velocities with fixed and scaled values of ODT parameter C (C_0 and C_{scal}, respectively).

Re_τ (Case)	η [mm]	$\frac{\partial \overline{p}}{\partial x}$ [Pa/m]	$U_{b,DNS}$ [m/s]	$U_{b,ODT}$ C_0 [m/s]	$U_{b,ODT}$ C_{scal} [m/s]
108 (0)	0.185	-0.555	1.16	1.29	1.29
108 (A)	0.185	-0.555	1.19	1.34	1.37
108 (B)	0.185	-0.555	1.23	1.44	1.56

EHD EFFECTS ON A LOW REYNOLDS CHANNEL FLOW

For EBFs which are independent of the flow whilst being functions of space and time, the predominant characteristic is the induction of mean flows, with their own eddy structures and oscillations, as detailed by Hunt (1995). This translates directly into a drag increase or reduction. Here, we analyze the changes in drag by analyzing both the mean velocity profiles and the Reynolds stress as shown in Figures 3a and 3b, respectively. Note that the cross-wise Reynolds stress in ODT is calculated following Kerstein (1999). For the same incompressible channel flow ODT model parameters C and Z, we observe an enhancement of the mean velocity gradient in the outer layer and a subsequent increase in the bulk velocity, as shown in Table 2 and seen in Figure 3a. We also note the increased probability of eddy events happening close to the electrodes due to the influence of the EBF, as seen in Figure 4. We note, though, that the difference between cases 0 and A is almost negligible in terms of the mean velocity profile for ODT. Also, the trends obtained in the Reynolds' stress are inverted in comparison to the results obtained in the DNS, as seen in Figure 3b. In ODT, the Reynolds stress increases with the magnitude of the EBF, while the opposite happens in the DNS. In fact, Soldati & Banerjee (1998) attribute the decrease of the Reynolds stress with the drag reduction experienced at larger EBF.

As detailed by Hunt (1995), changes in drag could be mainly attributed to the EBF induced mean flows. ODT is not able to capture coherent information that may lead to the induction of mean flows due to its reduced dimensionality, see Kerstein (1999). Therefore, we look for a way to influence the drag by changing the ODT C parameter. This could be similar to the C parameter dependency in ODT for low Reynolds number flows, where lower values of C reproduce more laminar flows ($C = 0$ reproduces a laminar channel flow). With this consideration, we treat the drag reduction as a laminarization of the flow, and thus, as a reduction in the C parameter, which should be a function of the EBF magnitude.

Reviewing the non-dimensional momentum equation detailed in Davidson & Shaughnessy (1986), we note that the EBF present in the momentum equation is non-dimensionalized by the parameter $Fr_{EHD}^{-2} = N_{EHD} = I_{plate}/\left(\rho b U_{b,0}^2\right)$, i.e. an electric Froude number. We have empirically found, that an appropriate qualitative behavior for the drag reduction and the Reynolds stress close to the wall, can be found by scaling the C

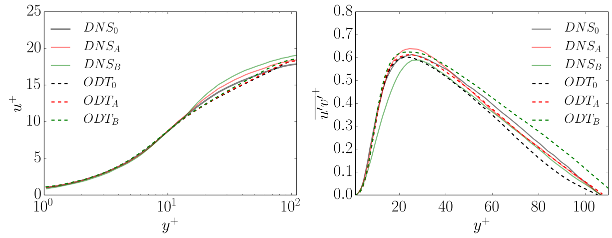

(a) (b)

Figure 3: Normalized mean velocity profile and Reynolds stress obtained with the ODT model parameters $C = 1.5$ and $Z = 100$.

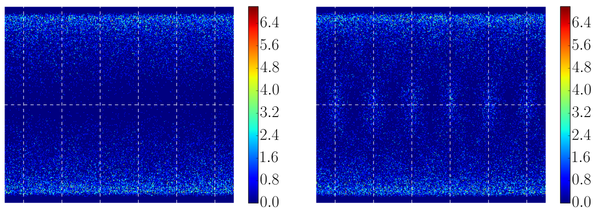

(a) (b)

Figure 4: Eddy event distribution in the plate ESP. (a) Case 0, no EBF. (b) Case B, large EBF. The different colors in the plots indicate the number of events. The intersection of the white dashed lines indicate the presence of the electrodes.

parameter as a direct function of N_{EHD},

$$C_{scal} = C_0 \left(1 - \frac{4}{27} N_{EHD} \right) \tag{11}$$

The factor $\frac{4}{27}$ appears here again, as in Eq. (7), indicating that C may be related to some energy contribution in the flow. Since C is related to the turbulence intensity, we hypothesize then that this modification of C may account for the missing mean kinetic energy introduced by the large scale structures (see mean kinetic energy equation in Davidson & Shaughnessy (1986)), which results in the noted reduction of the drag. Given the net cancellation effect of the EBF in the streamwise direction for a fully developed and statistically homogeneous flow, there is no direct way in ODT to feed this energy into the system, given our restraint regarding the 1-D (trivial) divergence condition, instead of the 2-D (or 3-D) velocity divergence condition, which is characteristic of an elliptic flow. We note that Eq. (11) might produce negative C values for sufficiently high N_{EHD}. This sets a limit for the S-ODT parabolic treatment, beyond which the solutions become indistinguishable from the pure still (no mean flow) EHD solution, given the complete absence of turbulent transport (eddy events). Using the suggested scaling, we can obtain a better distinction between cases 0 and A in the mean velocity profiles, while also obtaining the same DNS trends in the Reynolds stress close to the wall. For $N_{EHD,A} \approx 0.91$ we obtain $C_{scal,A} \approx 1.3$ and for $N_{EHD,B} \approx 2.28$ we obtain $C_{scal,B} \approx 1$. Despite the improvement of the behavior close to the wall, the qualitative disagreement of the Reynolds stress in the outer layer still persists. See Figures 5a and 5b for details.

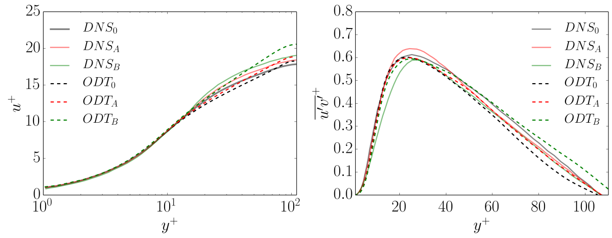

(a) (b)

Figure 5: Normalized mean velocity profile and Reynolds stress obtained with the ODT model parameter $Z = 100$ and the C parameter scaled according to Eq. (11).

Figure 6a shows the non-dimensional mean shear stress obtained with the scaled C parameter values in the low and high N_{EHD} cases. We note that ODT is able to reproduce the increase in the mean velocity gradient in the buffer layer for increasing magnitudes of the EBF. Although the trends are different than in the DNS, we note that the increase in the mean velocity gradient up to a position $y^+ \sim 30$ is contrasted with the decrease in the Reynolds shear stress. This is a feature reproduced in ODT, which would not be attainable with the classical Boussinesq turbulent viscosity approach.

In order to analyze the RMS velocity profiles and part of the TKE budgets, we perform a triple decomposition of the velocity field as in Soldati & Banerjee (1998),

$$u(x,y,n) = \overline{u}(y) + \langle u \rangle(x,y) + u'(x,y,n) \tag{12}$$

Here, $\overline{u}$ is the average achieving the fully developed condition of the velocity field and $\langle u \rangle$ is an ensemble average corresponding to a periodic position n, i.e. our equivalent to the phase average in Soldati & Banerjee (1998). We note that, although $\langle v \rangle \neq 0$ in the DNS, our uncorrelated ensemble average produces $\langle v \rangle = 0$ and therefore we are unable to analyze organized motions of the non-streamwise velocity components (plus our inability to obtain a w velocity component). We also define $\widehat{u}(x,y) = \langle u \rangle(x,y) - \overline{u}(y)$ as in the DNS. We note, that $\overline{\widehat{u}} = 0$ and $\overline{\widehat{u}\widehat{u}} \neq 0$. Using these definitions, we show in Figure 6b the RMS streamwise velocity profiles. We note that between cases 0 and A, the streamwise turbulence intensity has approximately the same magnitude in ODT close to the wall, departing towards a reduced turbulence intensity away from the wall in case A, as in the DNS. For case B, we note that the turbulence intensity is increased near and away from the wall in comparison to cases 0 and A. A drop in turbulence intensities only takes place very close to the centerline region, unlike in the DNS, where an earlier decrease in the outer layer is observed. We focus here again, on the behavior close to the wall, due to the inability of ODT to capture most of the coherent, large scale organized motion.

Finally, we show in Figure 7 the TKE production and dissipation budgets, P and D, respectively. The TKE production is split into a mean flow gradient TKE term (classical term) and an organized flow gradient TKE term, P_{EHD} as in Soldati & Banerjee (1998). For the small scale dynamics, we obtain a similar behavior in ODT for the TKE production budget, but we miss the organized P_{EHD} budget term completely. Due to this reason, most of the dissipation close to the wall, originated by this large scale motion

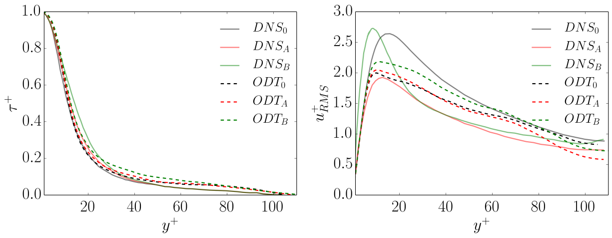

(a) (b)

Figure 6: Normalized mean shear stress and streamwise RMS velocity profile obtained with scaled ODT C parameter values.

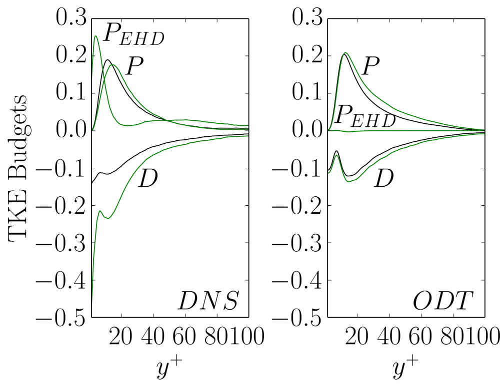

Figure 7: TKE production (P), dissipation (D), and EHD production (P_{EHD}) budgets. The left figure shows the DNS data for case 0 (black line) and case B (green line). The right figure shows the ODT results.

and dissipated at a different, larger scale (see Zhao & Wang (2017) for details), can not be matched by ODT. However, in general, we notice the characteristic increase in production and dissipation for the increased EBF.

CONCLUSIONS AND OUTLOOK

The effects of 2-D electrostatic fields on a low Reynolds channel flow were investigated. Although this work is the first step towards an ODT model formulation capable of accounting for EHD effects, we have corroborated some qualitative trends with the DNS of Soldati & Banerjee (1998). First of all, it is important to stress that the problem sketched in Fig. 1 is inherently three dimensional and a fully elliptic (boundary value) problem. The resulting flow shows very significant effects of recirculation, which can not be captured by our S-ODT parabolic formulation. We have, nonetheless, stated a formal pathway to mimic certain flow dynamics, considering only the rotational component of the electric current density. The latter is responsible for turbulence generation or decay, as stated by Davidson & Shaughnessy (1986).

As seen in the ODT and DNS results, an increase in the EBF results in an overall increase in turbulence, as proved by the increase in the TKE production and dissipation budgets, shown both in DNS and ODT. We also find a characteristic turbulence increase in ODT in the local zones of concentrated EBF, as seen by examining the 2-D eddy distribution in the ESP. Nevertheless, the 2-D EHD effects in the channel induce mean flow, mostly at the large scales and in the form of characteristic eddy structures. This increase in the mean kinetic energy results in a drag reduction, as well as a local relaminarization of the flow in the outer layer of the mean velocity profile. The drag reduction effect symbolized by the increase in the bulk velocity was confirmed with ODT. However, it was not possible to reproduce the kinetic energy of such characteristic eddy structures, due to the inability of ODT to capture coherent, large scale motion. Future studies will consider the cylindrical geometry of pipe ESPs, where the current density vector is expected to be fully irrotational. This represents a more dominant 1-D problem, from the body force point of view.

REFERENCES

Adamiak, K 2013 Numerical models in simulating wire-plate electrostatic precipitators: A review. *Journal of Electrostatics* **71** (4), 673–680.

Ashurst, Wm T & Kerstein, Alan R 2005 One-dimensional turbulence: Variable-density formulation and application to mixing layers. *Phys. Fluids* **17** (2), 025107.

Ashurst, Wm T & Kerstein, Alan R 2009 Erratum:one-dimensional turbulence: Variable-density formulation and application to mixing layers. *Phys. Fluids* **21** (11), 119901.

Atten, Pierre, McCluskey, Frank MJ & Lahjomri, Ahmed Chakib 1987 The electrohydrodynamic origin of turbulence in electrostatic precipitators. *IEEE Transactions on Industry Applications* (4), 705–711.

Davidson, Jane H & Shaughnessy, Edward J 1986 Turbulence generation by electric body forces. *Experiments in fluids* **4** (1), 17–26.

Hunt, JCR 1995 Effects of body forces on turbulence. In *Advances in Turbulence V*, pp. 229–235. Springer.

Jozefik, Z, Kerstein, A, Schmidt, H, Lyra, S, Kolla, H & Chen, J 2015 One-dimensional turbulence modeling of a turbulent counterflow flame with comparison to DNS. *Combust. Flame* **162**, 2999–3015.

Kerstein, A 1999 One-dimensional turbulence: model formulation and application to homogeneous turbulence, shear flows, and buoyant stratified flows. *J. Fluid Mech.* **392**, 277–334.

Kourmatzis, A & Shrimpton, JS 2018 Turbulence closure models for free electroconvection. *International Journal of Heat and Fluid Flow* **71**, 153–159.

Lignell, D, Kerstein, A, Sun, G & Monson, E 2013 Mesh adaption for efficient multiscale implementation of One-Dimensional Turbulence. *Theor. Comput. Fluid Dyn.* **27** (3-4), 273–295.

Panofsky, Wolfgang KH & Phillips, Melba 2005 *Classical electricity and magnetism*. Courier Corporation.

Schmid, Hans-Joachim & Vogel, Lutz 2003 On the modelling of the particle dynamics in electro-hydrodynamic flow-fields: I. comparison of eulerian and lagrangian modelling approach. *Powder Technology* **135**, 118–135.

Soldati, Alfredo & Banerjee, Sanjoy 1998 Turbulence modification by large-scale organized electrohydrodynamic flows. *Phys. Fluids* **10** (7), 1742–1756.

Yamamoto, Toshiaki 1979 Electrohydrodynamic secondary flow interaction in an electrostatic precipitator. PhD thesis, The Ohio State University.

Zhao, Wei & Wang, Guiren 2017 Scaling of velocity and scalar structure functions in ac electrokinetic turbulence. *Physical Review E* **95** (2), 023111.